nature cell biology

# Cell shape changes indicate a role for extrinsic tensile forces in *Drosophila* germ-band extension

**Lucy C. Butler[1,7], Guy B. Blanchard[1,7], Alexandre J. Kabla[2], Nicola J. Lawrence[3], David P. Welchman[4], L. Mahadevan[5,6], Richard J. Adams[1] and Benedicte Sanson[1,8]**

***Drosophila*** **germ-band extension (GBE) is an example of the convergence and extension movements that elongate and narrow embryonic tissues. To understand the collective cell behaviours underlying tissue morphogenesis, we have continuously quantified cell intercalation and cell shape change during GBE. We show that the fast, early phase of GBE depends on cell shape change in addition to cell intercalation. In antero-posterior patterning mutants such as those for the gap gene *Krüppel*, defective polarized cell intercalation is compensated for by an increase in antero-posterior cell elongation, such that the initial rate of extension remains the same. Spatio-temporal patterns of cell behaviours indicate that an antero-posterior tensile force deforms the germ band, causing the cells to change shape passively. The rate of antero-posterior cell elongation is reduced in *twist* mutant embryos, which lack mesoderm. We propose that cell shape change contributing to germ-band extension is a passive response to mechanical forces caused by the invaginating mesoderm.**

Convergence and extension movements remodel tissues during the morphogenesis of many embryos and organs, including vertebrate axis elongation[1–4]. During *Drosophila* gastrulation, the embryo trunk (the germ band) elongates in the antero-posterior (AP) axis and narrows in the dorso-ventral (DV) axis[5]. Polarized cell intercalation, which requires AP patterning, contributes to GBE[6–9]. However, the relative importance of cell intercalation versus other possible cell behaviours[10] has not been explained. Here we quantify the contribution of cell intercalation and cell shape change to tissue deformation in wild-type and mutant embryos.

We recorded the movement of up to 700 cells at 30-s intervals during GBE, imaging the ventral side of live *Drosophila* embryos (Fig. 1a). Cell outlines were labelled with *Drosophila* E–Cadherin–GFP[11], and cell movements were tracked and quantified with a theory and algorithms presented elsewhere[12] (Fig. 1a′, a′). To quantify local tissue deformation, domains defined by a central cell surrounded by a corona of neighbouring cells were followed over 2-min windows[12]. We quantified how fast each of these domains changed dimensions along the AP and the DV axes of the embryo ('total' strain rates). Next we quantified the average rates of shape change for cells belonging to each domain ('cell shape' strain rates). Finally, the strain rates attributable to cell intercalation were derived for each domain by subtracting the 'cell shape' strain rates from the 'total' strain rates (on the basis of the relationship total strain rate = cell shape strain rate + cell intercalation strain rate, defined in ref. 12). A strength of this method is that it provides a continuous measure of cell intercalation that encompasses every type of cell intercalation described so far in the germ band[6,7]. This measure also includes subtler cell intercalation movements that do not necessarily lead to cell neighbour exchange but nonetheless contribute to tissue deformation (Supplementary Information, Movie 1).

GBE proceeds rapidly for about 30 min (the fast phase), then continues at a slower rate for a further 90 min (the slow phase)[8,13]. GBE has been shown to require cell intercalation, but it is not clear why the extension rate is biphasic[6–10]. To understand this, we analysed five movies of wild-type embryos during the first 50 min of GBE. We confirmed that cell intercalation contributed to extension throughout the period analysed (Fig. 1b, c). However, we also found that cell shape change contributed to the first 30 min of GBE, with the peak contribution of cell shape change, at about 10 min, coinciding with the peak rate of tissue extension (Fig. 1b). Over these first 30 min, cell shape change contributed about one-third of total tissue deformation, identifying cell shape as a novel and significant contributor to GBE (Fig. 1c). We conclude that this additional contribution of cell shape change explains the higher rate of extension that distinguishes the fast phase from the slow phase.

Mutants in which AP patterning is defective, such as those for the gap gene *Krüppel*, do not extend their germ bands fully[6–9]. However, in all AP patterning mutants examined, normal tissue extension occurs initially, even though polarized cell intercalation is defective[8]. To understand this apparent contradiction we analysed five movies of *Krüppel*$^-$ embryos and found that in the

[1]Department of Physiology, Development and Neuroscience, University of Cambridge, Downing Street, Cambridge CB2 3DY, UK. [2]Engineering Department, University of Cambridge, Trumpington Street, Cambridge CB2 1PZ, UK. [3]Gurdon Institute, University of Cambridge, Tennis Court Road, Cambridge CB2 1QN, UK. [4]Global Health Institute, École Polytechnique Fédérale de Lausanne, CH-1015 Lausanne, Switzerland. [5]School of Engineering and Applied Sciences, Harvard University, Cambridge, Massachusetts 02138, USA. [6]Department of Systems Biology, Harvard Medical School, Boston, Massachusetts 02115, USA.
[7]These two authors contributed equally to the work.
[8]Correspondence should be addressed to B.S. (e-mail: bs251@cam.ac.uk)

Received 9 February 2009; accepted 28 April 2009; published online 7 June 2009; DOI:10.1038/ncb1894

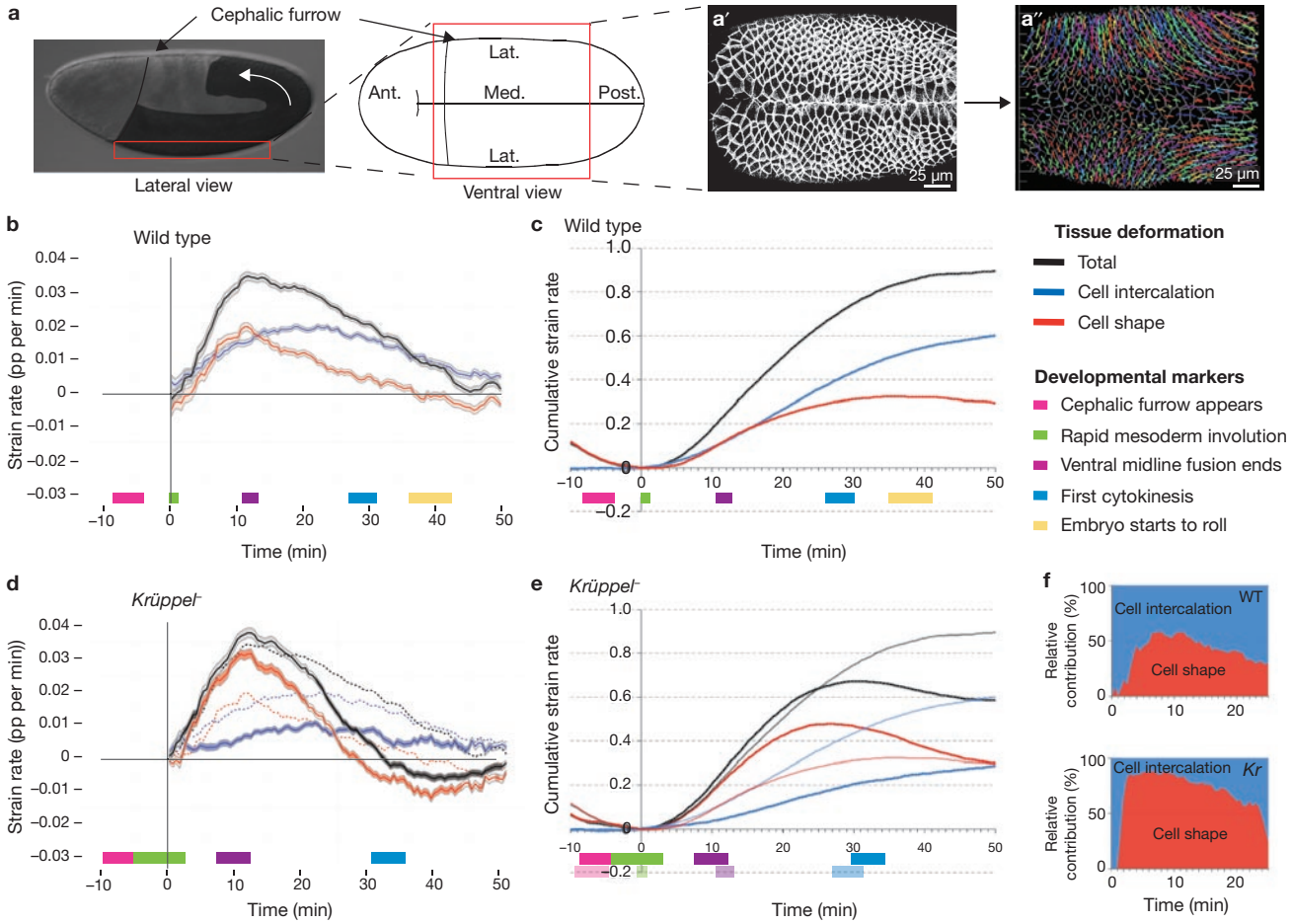


**Figure 1** Relative contribution of cell shape change and cell intercalation to germ-band extension in wild-type and *Krüppel*⁻ embryos. (**a**) Lateral view of a *Drosophila* embryo: the extending germ band is shaded (anterior to the left, dorsal uppermost). The red box indicates the stack of optical sections taken by confocal imaging, which corresponds to the ventral field of view shown in the adjacent panel. The left-hand side of the field of view is positioned with the cephalic furrow as a landmark. (**a′**) Corresponding movie frame showing a projection of confocal sections through the cell apices labelled with *DEcadGFP* (Methods). The midline bisecting the embryo is the closing furrow through which the mesoderm has invaginated. (**a″**) Tracked movie frame showing the cell lineages (tracks), cell centroids (endpoints of tracks) and cell outlines recorded by the tracking software. (**b**) Summary of deformation (strain) rates in the AP axis for five wild-type embryos, showing total, cell intercalation and cell shape strain rates (see key). A strain rate is the ratio of the change in length to the original length, divided by the time interval, with units of proportion (pp) per minute. The lines show the mean strain rates for all five embryos, and the ribbon width represents the average standard error within a data set. The timing of developmental landmarks is shown for the five embryos recorded. (**c**) Cumulative representation of the same data, accumulating from $t = 0$. (**d**) Tissue deformation in the AP axis for five homozygous *Krüppel*⁻ embryos. Dotted lines show the wild-type data for comparison. The shaded sections of the ribbons indicate when a given cell behaviour in the mutant was significantly different from the equivalent at that time in the wild type ($P < 0.05$). (**e**) Cumulative representation of the same data; for comparison, wild-type curves are shown as a lighter coloured line, and wild-type developmental landmarks as lighter coloured boxes on the same graph. (**f**) Relative instantaneous contribution of cell shape changes and cell intercalation to extension in wild-type (WT) and *Krüppel*⁻ (*Kr*) mutant embryos, for the first 25 min of germ-band extension, which corresponds to the period when the total extension rate is the same in both genotypes.

first 25 min of GBE, although the rate of cell intercalation was decreased, the rate of cell shape change was increased (Fig. 1d). This increased rate of cell shape change compensated fully for the loss of cell intercalation, resulting in an initial rate of tissue extension indistinguishable from that of the wild type (Fig. 1e), with cell shape change now accounting for most of the tissue extension (Fig. 1f). We found a similar compensation when analysing two other AP patterning mutants: a mutant in the pair-rule gene *even-skipped* (*eve*), and a double mutant in the gap genes *knirps* and *hunchback* (*kni hb*) (Supplementary Information, Fig. 3). Because these analyses were conducted for the whole field of view, we confirmed them by examining the ectodermal cell population alone (Fig. 2a). In the mutant ectoderms, cell intercalation rates were either reduced (*eve* and *kr* mutants) or abolished (*kni hb*), whereas cell shape change was systematically increased compared with that of the wild type (Fig. 2b–d). Increased cell shape change therefore explains the maintenance of an initial rapid rate of tissue extension in AP mutants with defective cell intercalation[8].

Our results indicate that an unidentified mechanism independent of AP patterning or polarized cell intercalation causes cell shape change in the germ band. Cell shape change could be cell-autonomously controlled by a genetic program acting independently of AP patterning. However, this would not explain why cell shape change increases when polarized cell intercalation decreases in AP-patterning mutants. A more plausible scenario is that in both wild-type and AP mutants, an external force is acting on the germ-band cells, causing them to change shape passively in response to tension[14]. We propose that autonomous polarized cell intercalation relaxes the stress imposed on the germ-band tissue by this external

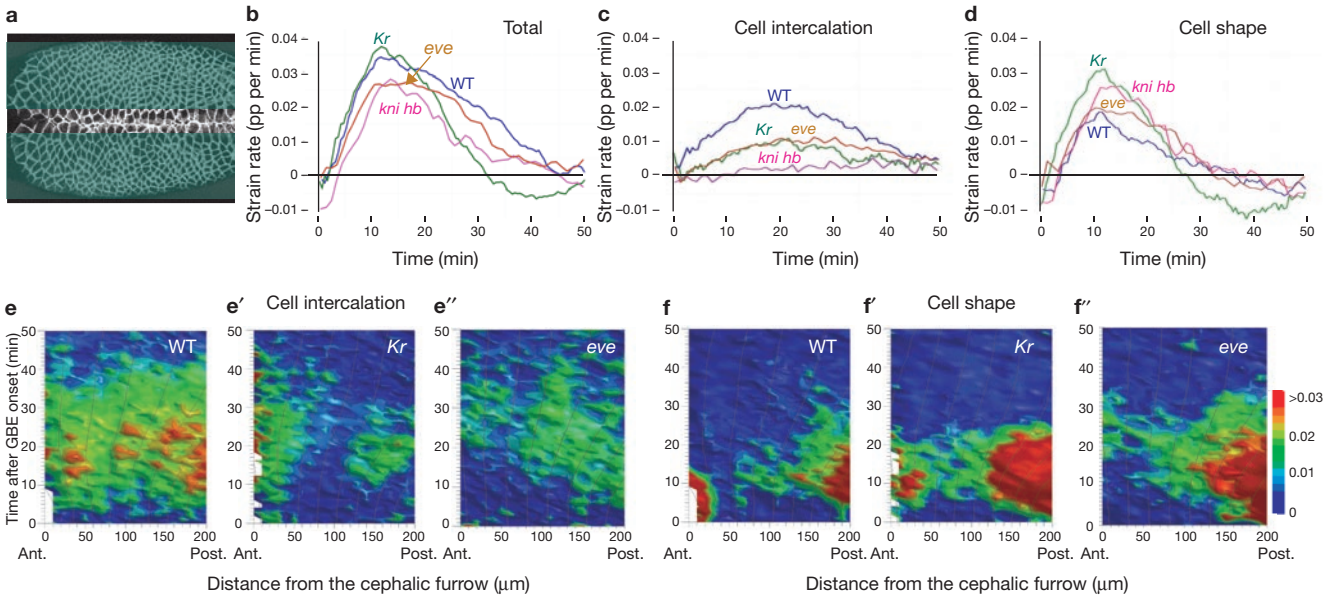


**Figure 2** Spatio-temporal analysis of cell behaviours in the ectoderm of wild-type and AP patterning mutant embryos. (**a**) The field of view that we analyse contains a mixture of ectodermal cells (laterally) and mesectodermal cells (at the ventral midline). The ectodermal cells (shaded areas) were selected for further analysis. (**b**–**d**) Comparison of the strain rates in the AP axis for total tissue (**b**), cell intercalation (**c**) and cell shape (**d**), for the wild type (WT) and three AP patterning mutants, *even-skipped* (*eve*), *Krüppel* (*Kr*) and *knirps hunchback* (*kni hb*). Lines show the mean strain rate (pp, proportion) for the ectodermal cells for five embryos (WT, *Kr* and *eve*) or a single embryo for *kni hb*. (**e**–**e**′) Strain rates for cell intercalation contributing to tissue extension in WT (**e**), *Kr*$^-$ (**e**′) and *eve*$^-$ (**e**′′) embryos (average for five embryos of each genotype), represented as a function of the cell's position along the AP axis. Strain rates are colour-coded in accordance with the scale shown (note that any values below 0 are coded blue, and any above 0.03 are coded red). Cell position is given in micrometres from the anterior cephalic furrow (or corresponding position for *eve*$^-$), which separates head from trunk tissue (see Fig. 1a). The tissue is moving with respect to the cephalic furrow as it extends in the AP axis, and the overlaid black lines follow this translation of the tissue over time. The data are shown here for the ectodermal cell population only. (**f**–**f**′′) Similar analysis for cell shape strain rates.

force. In AP-patterning mutant embryos, this dissipation is decreased because cell intercalation is defective, and cell shape change increases.

To investigate this further, we looked at variations in cell behaviour along the AP axis in the ectoderm of wild-type and AP-patterning mutant embryos (Fig. 2e–f′′). Cell intercalation rates were mostly uniform along this axis in wild-type embryos (Fig. 2e). In *kni hb* embryos, which lack AP patterning in the trunk, cell intercalation was abolished throughout the field of view, as expected (Supplementary Information, Fig. 3g). In *Krüppel*$^-$ embryos, cell intercalation was abolished in a central region, and decreased elsewhere (Fig. 2e′). This pattern is consistent with a loss of cell intercalation where *Krüppel* is normally expressed, and a weaker trunk-wide effect, perhaps due to mis-expression of pair-rule genes in the *Krüppel*$^-$ mutant. Planar polarization of myosin II is associated with polarized cell intercalation in the germ band[6,7,9]. Consistent with this was our observation that myosin II concentration at the apical cell cortex was decreased in the ventral ectoderm of *Krüppel*$^-$ mutant embryos (data not shown). Note that we did not detect a difference in myosin II localization between the central and posterior domain to explain the observed difference in cell intercalation rates (Fig. 2e′). In *even-skipped*$^-$ embryos, cell intercalation was decreased uniformly along the length of the trunk (Fig. 2e′), which is consistent with *eve* expression in seven closely spaced stripes.

The pattern of cell shape change in wild-type embryos was graded along the AP axis, increasing from the centre towards the posterior end of the embryo between 5 and 20 min of GBE (Fig. 2f). There was also a shorter pulse of cell elongation at the anterior end for the first 15 min of GBE, which was also present in *Krüppel* embryos (Fig. 2f′) but absent from *even-skipped*$^-$ embryos (Fig. 2f′). This suggests that anterior cell elongation is a consequence of cephalic furrow formation, which is defective in *eve* mutants[15] (Supplementary Information, Fig. 3a). In both *Krüppel*$^-$ and *even-skipped* mutants (and also in *kni hb* mutants; Supplementary Information, Fig. 3h), the central to posterior gradient of cell elongation was maintained but the rate of cell shape change was increased (Fig. 2f′, f′′). The presence of a gradient of AP cell elongation in wild-type and all AP mutants examined supports the idea that cell shape change is a passive response to the same extrinsic force.

This extrinsic force could be an AP pulling force or a DV pushing force. To investigate this, we examined the posterior domain of the germ band in *Krüppel*$^-$ mutants, a region with strong deformation (Fig. 3a–c). If cells deform passively in response to mechanical forces, they should behave qualitatively like a passive cellular material such as a foam, in which shape reflects stress[16]. Accordingly, different signatures are expected for pulls or pushes: if the tissue experiences a pull in one direction, it will tend to contract in the other two axes, leading to an increase in the cell projected area. Conversely if the tissue is compressed (for instance in the DV axis), cell area is expected to decrease. We found an increase in apical cell area as cells elongated in the posterior tissue of *Krüppel*$^-$ embryos (Fig. 3d, d′; see also Fig. 3e), suggesting that AP cell elongation in this domain results from an AP pull rather than a DV compression.

The analyses of cell shape and cell area also showed that, 10 min after GBE initiation, cells in wild-type embryos acquired an isometric apical shape that they maintained for the remainder of GBE (Fig. 3d, e). In *Krüppel*$^-$ mutants, however, cell shapes were briefly isometric at about 10 min then became elongated in the AP axis (Fig. 3d′, e). We propose that in wild-type embryos, autonomous polarized cell intercalation relaxes the stress imposed externally on the germ band, allowing stretched cells to return to isometric shapes. In *Krüppel*$^-$ embryos, the

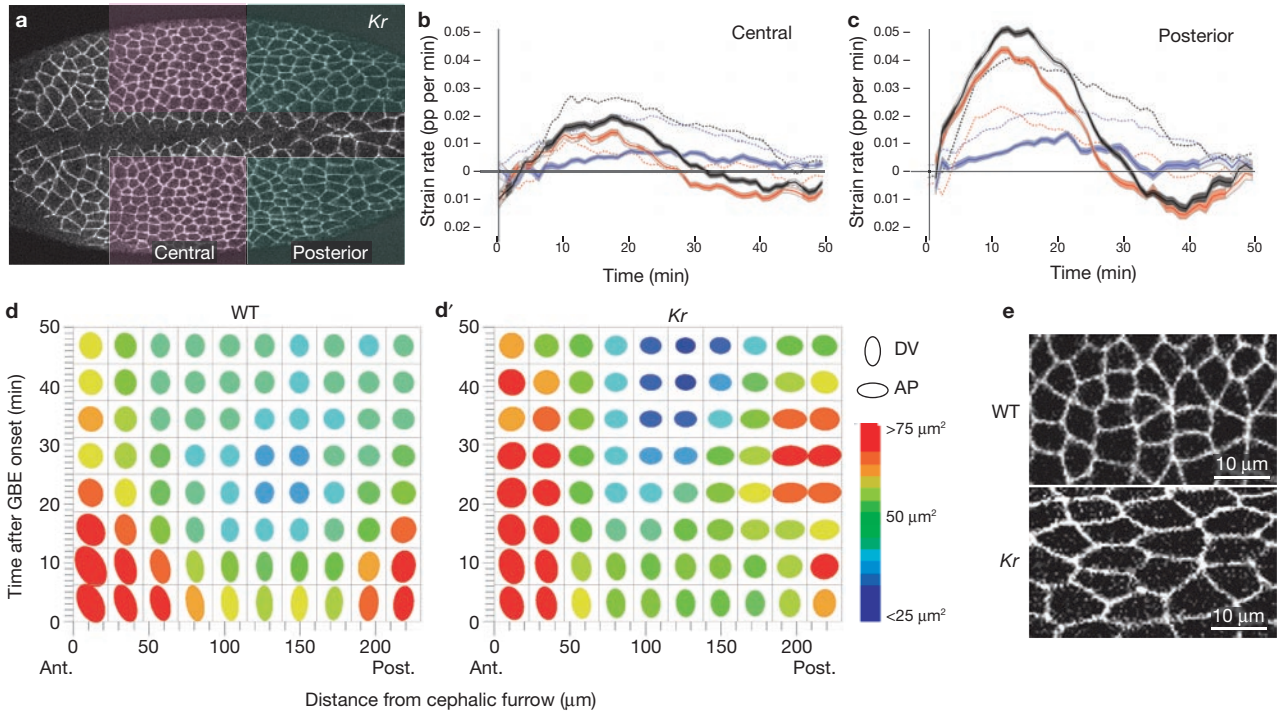


**Figure 3** Spatio-temporal analysis of cell shape and cell area change in the ectoderm of wild-type and *Krüppel*⁻ embryos. (**a**) The central and posterior ectodermal cell populations (shaded areas) were analysed separately (see also Supplementary Information, Fig. 3i, j). (**b**, **c**) Strain rates in the AP axis for total (black), cell intercalation (blue) and cell shape (red), for the central (**b**) and posterior (**c**) populations of ectodermal cells in wild-type (WT) and *Krüppel*⁻ embryos (pp, proportion). Wild-type is shown as dotted lines and *Krüppel*⁻ as a ribbon, with ribbon shading indicating a significant difference between the two genotypes ($P < 0.05$). (**d**, **d**′) Representation of the average cell shape, cell area (quantified by colour coded scale) and cell orientation (see key), in accordance with the cell's position along the AP axis (cell positions are given in μm from cephalic furrow) and time. Note that ectodermal cells only are analysed in wild-type (**d**) and *Krüppel*⁻ (**d**′) embryos. After 10 min of GBE, the WT germ-band cells acquire an isotropic shape and maintain it, whereas the cells elongate in the AP orientation in *Krüppel*⁻ mutants, especially at the posterior, where cell area is also greatest at this time. (**e**) Close-up of movie frames of WT and *Krüppel*⁻ embryos at mid-extension in the posterior domain, showing that whereas WT cells retain an isotropic shape, mutant cells are visibly elongated in the AP axis.

decrease in polarized intercalation caused by the defect in AP patterning upsets this balance, and cells stretch passively in the AP axis in response to tension. When this tension ceases, at about 25 min into GBE, the cells contract back for another 25 min, suggesting that the tissue relaxes as in an elastic response (Fig. 3c; see also Fig. 1d).

Other morphogenetic movements happening concurrently with GBE are good candidates for causing an AP tensile force. The sharp increase in the rate of cell shape change at the beginning of GBE overlaps with mesoderm invagination (Fig. 1b, d). Because *twist* is required for mesoderm specification and invagination[5,17–19], we analysed five movies of *twist*⁻ mutant embryos (Fig. 4). Mesoderm invagination causes the cells on both sides of the furrow to become elongated towards the midline[5,11,20,21] (see also Fig. 3d, d′). The peak of cell elongation in the DV axis, which was lost as expected in *twist*⁻ mutants (Fig. 4a′; see also Fig. 4f), was tightly temporally correlated with the onset of GBE (Fig. 4a; Supplementary Information, Fig. 1). Moreover, in *twist*⁻ embryos, in which mesoderm invagination failed, the rates of both cell shape and cell intercalation strains in the AP axis were decreased in the first 20 min of GBE (Fig. 4b, c), even though *twist*⁻ mutants ultimately extended their germ bands as far as those in the wild type[8] (Supplementary Information, Fig. 2). This indicates that *twist* is required for the fast rate of extension at the beginning of GBE. In contrast to the wild type, small, non-invaginated 'mesodermal' cells are present in the field of view in *twist*⁻ mutants. To compare the same population of cells in *twist*⁻ mutants and the wild type, we analysed the ectodermal cell population alone and confirmed these results (Fig. 2a; Supplementary Information, Fig. 4a, b). Given that ectodermal cells do not express *twist*, this demonstrates an indirect (non-cell-autonomous) requirement for *twist* in the fast phase of GBE.

Cell intercalation in *twist*⁻ mutants was decreased almost uniformly along the AP axis (Fig. 4d), but cell shape change was not (Fig. 4e). The anterior pulse of cell elongation was maintained, as expected because *twist* mutants have normal cephalic furrows, but the steep gradient of cell shape change towards the posterior was substantially reduced. Thus, *twist* is required non cell-autonomously for cell shape change that is patterned in the AP axis. Because *twist* is not known to regulate AP patterning[5,22,23], this suggests that the gradient of cell shape change and the AP tensile force depends on the invaginating mesoderm itself. Moreover, ectodermal cells in *twist*⁻ embryos maintained an isometric shape throughout extension despite decreased cell intercalation (Fig. 4f), which is consistent with the hypothesis that the tensile force is attenuated in this mutant.

The non-invaginated 'mesodermal' cells in *twist* mutants could act as a brake and decrease an AP tensile force generated by morphogenetic movements elsewhere in the embryo. Alternatively, the invaginating mesoderm could be the direct cause of the AP tensile force deforming the germ band in the fast phase. Note that AP cell elongation in wild-type and AP-patterning mutant embryos might also result from a relaxation of the ectoderm stretched along the DV axis during mesoderm invagination. However, tissue relaxation is unlikely to explain the observed

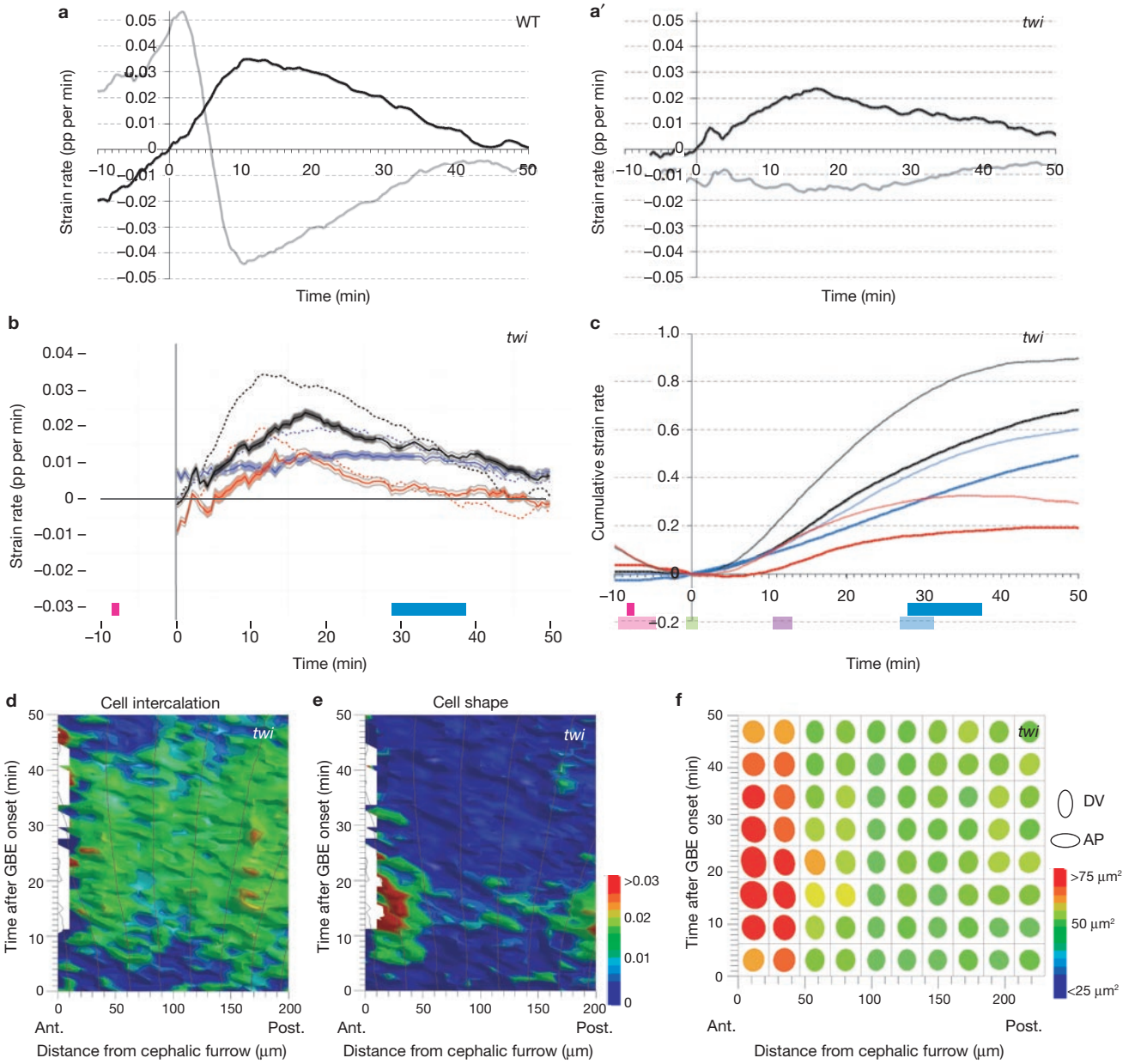


**Figure 4** Relationship between mesoderm invagination and germ-band extension. (**a**) Tissue deformation in the DV axis (convergence, grey) and the AP axis (extension, black) in wild-type (WT) embryos. The tissue deformation peak in the DV axis at the onset of germ-band extension corresponds to the ventrolateral tissue stretching in the DV axis in response to mesoderm invagination (pp, proportion). (**a′**) As expected, this peak of DV stretching is absent in *twist*⁻ (*twi*) embryos. (**b**) Tissue deformation in the AP axis for five homozygous *twist*⁻ embryos in which there is no mesodermal invagination (total strain rate in black, cell shape in red, cell intercalation in blue). Dotted lines show the wild-type data for comparison. Ribbon shading indicates a significant difference between mutant and wild type ($P < 0.05$). (**c**) Cumulative representation of the same data, with lighter colours for corresponding wild-type data. (**d**) Strain rates for cell intercalation contributing to tissue extension in *twist*⁻ embryos are represented as a function of the cell's position along the AP axis. (**e**) Similar analysis for cell shape strain rates. (**f**) Representation of averages for cell shape, area and orientation, along the AP axis and throughout germ-band extension for *twist*⁻ embryos.

increase in cell area and cell elongation in the posterior of the germ band, suggesting that an AP tensile force predominates here.

Aside from mesoderm invagination, three other morphogenetic movements could conceivably produce the force deforming the germ band: cephalic furrow formation, posterior midgut invagination and amnioserosa cell elongation. Although cephalic furrow formation is correlated with the pulse of cell elongation in the anterior domain (Fig. 2f–f′′), the central-to-posterior gradient of cell elongation is intact in *eve* mutants, which do not have cephalic furrows. Posterior midgut invagination, which initiates on the dorsal posterior side, could pull the ectodermal tissue around the posterior of the embryo[5]. However, analysis of extension rates in a *folded gastrulation* (*fog*) mutant, which blocks the formation of posterior midgut invagination[19], shows that tissue deformation, cell intercalation and cell shape change are indistinguishable from those in the wild type during the first 20 min of extension (Supplementary Information, Fig. 5). Finally,

DV elongation of the amnioserosa cells on the dorsal side[24] could push the ectodermal tissue towards the midline. However, cell area measurements suggest that AP tension rather than DV compression explains cell deformation in the posterior domain (see Fig. 3d′, e). Given the above, we propose that mesoderm invagination is the main source of AP tensile force.

In support of a direct role for the invaginating mesoderm, we found that the germ band extends fastest close to the midline during the fast phase, suggesting an axial pull (Supplementary Information, Fig. 4c, d). A possible mechanism is that, once invaginated, the mesoderm undergoes convergence and extension (through an AP-patterning-independent mechanism), elongating the tube in the AP axis. This convergence and extension of the mesoderm (which is consistent with earlier observations[5,19]) could drag the midline cells and adjacent ectodermal tissue, as reported for amphibian gastrulation[14,25].

In summary, we have found, in contrast to what was previously thought[6,8,13], that cell shape change contributes significantly to the fast phase of germ-band extension. Whereas cell intercalation during GBE requires AP patterning[6–9], cell shape change is under the control of DV patterning, because it is decreased in *twist*$^{-}$ mutants. Our analysis of cell shape change and cell intercalation shows that at the beginning of the fast phase, the decrease in cell intercalation in AP mutants is compensated for by an increase in AP cell elongation such that the overall rate of tissue extension can initially remain the same. These findings parallel our earlier observations on notochord extension in zebrafish[1], another tissue previously thought to extend as a sole consequence of active convergence. In both studies, quantitative analyses reveal redundancy in the forces extending the body axis, highlighting the robustness of convergence and extension movements.

We propose that cell shape change is a passive response to an AP tensile force resulting from convergence and extension of the internalizing mesoderm. Intriguingly, in addition to a decrease in the rate of cell shape change, the rate of intercalation is decreased by about 30% in the first 25 min of GBE in *twist*$^{-}$ mutants (Fig. 4b, c; Supplementary Information, Fig. 4a), even though the AP patterning system on which the polarized exchange of cell neighbours depends is not affected in *twist*$^{-}$ mutants[5,8]. One possible explanation is that the AP tensile force that normally stretches the ectodermal cells also increases the rate of polarized cell intercalation. Stretching cells in the AP axis could make it mechanically favourable for cell junctions to shorten in the orthogonal DV axis, as suggested previously[26,27]. DV junction shortening is the first step leading to cell neighbour exchange in the germ band[6,7]. Thus, our analysis provides an opportunity to explore how the autonomous cell behaviours described previously[6–9] interact with mechanical forces generated by morphogenetic movements[14].

## METHODS

Methods and any associated references are available in the online version of the paper at http://www.nature.com/naturecellbiology/

*Note: Supplementary Information is available on the Nature Cell Biology website.*

ACKNOWLEDGEMENTS

We thank Claire Lye, Bruno Monier and Daniel St Johnston for comments on the manuscript and discussions. We thank the Bloomington Drosophila Stock Centre for fly strains. This work was supported by a Human Frontier Science Program grant to B.S., a Wellcome Trust studentship to L.C.B., a Medical Research Council grant to R.J.A. and a Harvard–National Science Foundation Materials Research Science and Engineering Center award to M.L.

AUTHOR CONTRIBUTIONS

This project grew from a close collaboration between the groups of B.S. and R.J.A. L.C.B. performed the experiments and analysed the data with G.B.B., R.J.A. and B.S. N.J.L. performed the initial experiments and developed the time-lapse methods. D.P.W. contributed to experiments and manuscript preparation. Strain rate analyses were developed by G.B.B., A.J.K., R.J.A. and L.M., building on a tracking and quantification framework of G.B.B. and R.J.A. B.S. and L.C.B. designed the *Drosophila* experiments and prepared the manuscript. All authors contributed to data interpretation and editing of the manuscript.

COMPETING FINANCIAL INTERESTS

The authors declare that they have no competing financial interests.

Published online at http://www.nature.com/naturecellbiology
Reprints and permissions information is available online at http://npg.nature.com/reprintsandpermissions/

1. Glickman, N. S., Kimmel, C. B., Jones, M. A. & Adams, R. J. Shaping the zebrafish notochord. *Development* **130,** 873–887 (2003).
2. Keller, R. Mechanisms of elongation in embryogenesis. *Development* **133,** 2291–2302 (2006).
3. Solnica-Krezel, L. Conserved patterns of cell movements during vertebrate gastrulation. *Curr. Biol.* **15**, R213–R228 (2005).
4. Munro, E. M. & Odell, G. M. Polarized basolateral cell motility underlies invagination and convergent extension of the ascidian notochord. *Development* **129,** 13–24 (2002).
5. Costa, M., Sweeton, D. & Wieschaus, E. Gastrulation in *Drosophila*: Cellular mechanisms of morphogenetic movements in *The development of Drosophila melanogaster* (eds. Bate, M. & Martinez-Arias, A.) 425–465 (Cold Spring Harbor Laboratory Press, 1993).
6. Bertet, C., Sulak, L. & Lecuit, T. Myosin-dependent junction remodelling controls planar cell intercalation and axis elongation. *Nature* **429,** 667–671 (2004).
7. Blankenship, J. T., Backovic, S. T., Sanny, J. S., Weitz, O. & Zallen, J. A. Multicellular rosette formation links planar cell polarity to tissue morphogenesis. *Dev. Cell* **11,** 459–470 (2006).
8. Irvine, K. D. & Wieschaus, E. Cell intercalation during *Drosophila* germband extension and its regulation by pair-rule segmentation genes. *Development* **120,** 827–841 (1994).
9. Zallen, J. A. & Wieschaus, E. Patterned gene expression directs bipolar planar polarity in *Drosophila*. *Dev. Cell* **6,** 343–355 (2004).
10. da Silva, S. M. & Vincent, J. P. Oriented cell divisions in the extending germband of *Drosophila*. *Development* **134,** 3049–3054 (2007).
11. Oda, H. & Tsukita, S. Real-time imaging of cell–cell adherens junctions reveals that *Drosophila* mesoderm invagination begins with two phases of apical constriction of cells. *J. Cell Sci.* **114,** 493–501 (2001).
12. Blanchard, G. B. *et al.* Tissue tectonics: morphogenetic strain rates, cell shape change and intercalation. *Nature Methods* **6,** 458–464 (2009).
13. Hartenstein, V. & Campos-Ortega, J. A. Fate-mapping in wild-type *Drosophila melanogaster*. 1. The spatio-temporal pattern of embryonic cell divisions. *Roux' Arch. Dev. Biol.* **194,** 181–195 (1985).
14. Keller, R., Shook, D. & Skoglund, P. The forces that shape embryos: physical aspects of convergent extension by cell intercalation. *Phys. Biol.* **5,** 15007 (2008).
15. Vincent, A., Blankenship, J. T. & Wieschaus, E. Integration of the head and trunk segmentation systems controls cephalic furrow formation in *Drosophila*. *Development* **124,** 3747–3754 (1997).
16. Weaire, D. & Hutzler, S. *The Physics of Foams* (Oxford Univ. Press, 2001).
17. Leptin, M. & Grunewald, B. Cell shape changes during gastrulation in *Drosophila*. *Development* **110,** 73–84 (1990).
18. Seher, T. C., Narasimha, M., Vogelsang, E. & Leptin, M. Analysis and reconstitution of the genetic cascade controlling early mesoderm morphogenesis in the *Drosophila* embryo. *Mech. Dev.* **124,** 167–179 (2007).
19. Sweeton, D., Parks, S., Costa, M. & Wieschaus, E. Gastrulation in *Drosophila*: the formation of the ventral furrow and posterior midgut invaginations. *Development* **112,** 775–789 (1991).
20. Kam, Z., Minden, J. S., Agard, D. A., Sedat, J. W. & Leptin, M. *Drosophila* gastrulation: analysis of cell shape changes in living embryos by three-dimensional fluorescence microscopy. *Development* **112,** 365–370 (1991).
21. Pouille, P. A. & Farge, E. Hydrodynamic simulation of multicellular embryo invagination. *Phys. Biol.* **5,** 15005 (2008).
22. Leptin, M. *twist* and *snail* as positive and negative regulators during *Drosophila* mesoderm development. *Genes Dev.* **5,** 1568–1576 (1991).
23. Thisse, B., Stoetzel, C., Gorostiza-Thisse, C. & Perrin-Schmitt, F. Sequence of the *twist* gene and nuclear localization of its protein in endomesodermal cells of early *Drosophila* embryos. *EMBO J.* **7,** 2175–2183 (1988).
24. Pope, K. L. & Harris, T. J. Control of cell flattening and junctional remodeling during squamous epithelial morphogenesis in *Drosophila*. *Development* **135,** 2227–2238 (2008).
25. Keller, R., Shih, J. & Sater, A. The cellular basis of the convergence and extension of the *Xenopus* neural plate. *Dev. Dyn.* **193,** 199–217 (1992).
26. Keller, R. E. & Trinkaus, J. P. Rearrangement of enveloping layer cells without disruption of the epithelial permeability barrier as a factor in *Fundulus* epiboly. *Dev. Biol.* **120,** 12–24 (1987).
27. Weliky, M. & Oster, G. The mechanical basis of cell rearrangement. I. Epithelial morphogenesis during *Fundulus* epiboly. *Development* **109,** 373–386 (1990).

## METHODS

**Fly strains.** Apical cell membranes were labelled with *ubi–DE–Cadherin–GFP* (abbreviated as *DEcadGFP*), a fusion between DE–Cadherin and GFP[11]. We used the null mutant alleles *eve[3], Kr[1]*, *kni[10]hb[4]*, *twist[1]* and *fog[S4]*. To label cells in these mutant backgrounds, we made the recombinant chromosomes *eve[3]DEcadGFP*, *Kr[1]DEcadGFP* and *twist[1]DEcadGFP* and the balanced stocks *DEcadGFP; kni[10]hb[4]* and *fog[S4]; DEcadGFP*.

**Movie acquisition.** Embryos at the end of cellularization were mounted on $O_2$-permeable membrane (Sartorius) and covered in Voltalef oil (Attachem). The embryo to be imaged was rolled to have the ventral side in the field of view, and the stage was rotated to capture the equivalent field of view for each embryo, with the cephalic furrow just visible to the left and the ventral furrow bisecting the field of view horizontally (Fig. 1a′). The tissue that undergoes polarized intercalation at gastrulation is the ventrolateral ectoderm, and this tissue is about 40 cell diameters long in the AP axis, and 20–23 cell diameters wide in the DV axis at the beginning of GBE[13]. Our field of view captures 12–15 cell diameters on each side of the invaginated mesoderm (midline) at the onset of GBE (Fig. 1a′; see also Supplementary Information, Movies 2–4). This corresponds to the ventralmost 60% of the ventrolateral ectoderm on each side of the midline. Homozygous mutant embryos were identified by the absence of GFP expression from the balancer chromosome *CyOKrGal4UASGFP*[28] and by their phenotypes. Note that *twist*-null mutants show variable mesoderm invagination defects that range from very shallow furrows to almost wild-type-like deep furrows[18]. To ensure a consistent phenotype, we analysed five *twi* mutant embryos exhibiting the most severe of these phenotypes. Movies were recorded at 20.5 ± 1 °C, measured with a high-resolution thermometer (Checktemp1). Time points were taken every 30 s on a MRC1024 Bio-Rad confocal microscope coupled to an upright Nikon Eclipse E800 microscope (with a 40× oil-immersion Plan/Fluor objective, numerical aperture 1.3). For each time point, a z-stack of ten optical slices separated by 1 μm were taken, starting from the apical surface of the cells (Supplementary Information, Movies 2–4). After each movie, embryos were left to develop, to check that they survived normally until the end of embryogenesis. For mutant embryos, the cuticle was mounted in Hoyer's medium to verify that it showed the expected phenotype.

**Movie tracking.** The confocal *Z*-stacks were converted into stacks of curved two-dimensional representations, the outermost of which followed the surface of the embryo. The section giving the clearest view of cell apices was selected for tracking. Tracking software identifies cells and links them in an iterative process using a watershedding algorithm[12]. For each cell at each time point, the program stores the coordinates of the centroid and also those of a polygon describing the cell, as well as information about the cell lineage (Supplementary Information, Movies 5–7).

**Movie analysis.** Using the relative movement of cell centroids, the strain rate for a small domain of tissue composed of one corona of cell neighbours is calculated for each cell and for each 2-min interval (corresponding to four movie frames)[12] (Supplementary Information, Movies 8–10). A direct measure of cell shape change is calculated by first approximating each cell from this small region to an ellipse, then finding the strain rates that best map a cell's elliptical shape as it evolves over time (Supplementary Information, Movies 11–13). The difference between the total strain rate and cell shape strain rate is attributed to cell intercalation[12] (Supplementary Information, Movies 14–16). These strain rates are then projected onto the embryonic axes, AP and DV. Cell area change is calculated as the mean of the AP and DV cell shape strain rates.

**Intragenotype movie synchronization.** Within the same genotype, movies were synchronized in most cases by making a quantitative comparison, using a given threshold of proportional change per minute for instantaneous proportional extension in the AP axis. We use a synchronization threshold of 0.01 for wild-type and *Krüppel*$^-$ and 0.005 for *twist*$^-$ embryos (which have a lower initial rate of extension). For *even-skipped*$^-$ embryos, we made a qualitative comparison, using the peaks of extension and convergence to synchronize the movies.

**Intergenotype movie synchronization.** Average strain rate curves weighted by planar cell area were calculated for each genotype. Genotypes were then synchronized using the zero time of average instantaneous extension in the AP axis. Note that, in contrast with mutant embryos analysed in this study, most wild-type embryos rolled on their sides during filming, about 40 min after the onset of germ-band extension (see Fig. 1b). Thus, the field of view in wild-type embryos incorporated progressively more lateral cells from this point onwards than in the mutants analysed.

**Statistical validation.** To test for evidence of differences between data derived from different embryos, we constructed a mixed-effects model[29] using R software[30]. We estimated the *P* value associated with a fixed effect of differences between genotypes, allowing for random effects contributed by differences between embryos within a given genotype. Error ribbons show the typical standard error for data from one embryo, averaged across all embryos of that group[31]. Sections of ribbons are shaded when $P < 0.05$, signifying evidence for a difference between genotypes.

28. Casso, D., Ramirez-Weber, F. A. & Kornberg, T. B. GFP-tagged balancer chromosomes for *Drosophila melanogaster*. *Mech. Dev.* **88,** 229–232 (1999).
29. Pinheiro, J. C. & Bates, D. M. *Mixed-effects Models in S and S-PLUS* (Springer, 2000).
30. R Research Development Team. *R: A language and environment for statistical computing*. (R Foundation for Statistical Computing, 2008).
31. Wickham, H. ggplot2: an implementation of the grammar of graphics. *R package version 0.8.1* (Springer, 2008).

nature cell biology



DOI: 10.1038/ncb1894

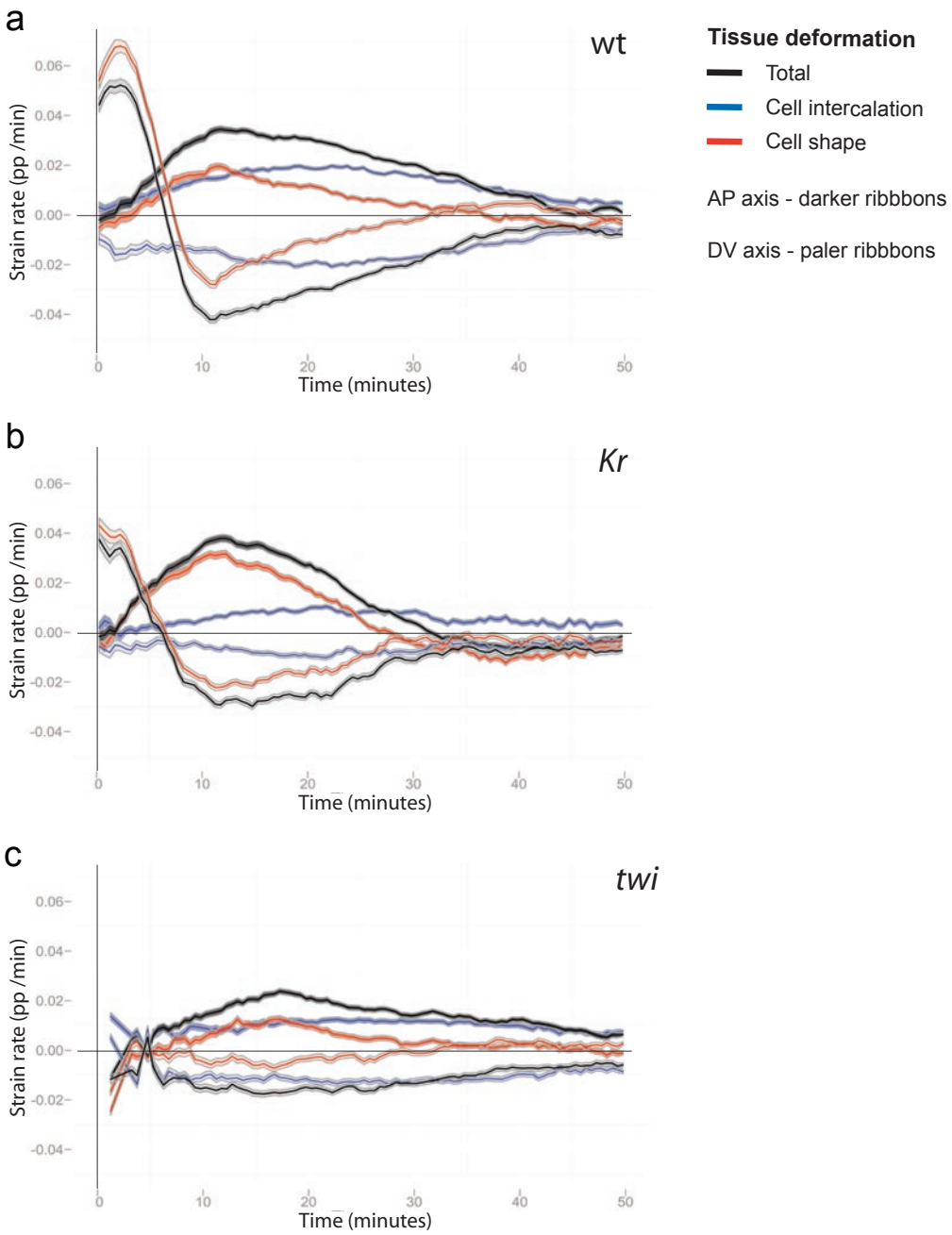


**Figure S1** Tissue deformation in the AP and DV embryonic axes for wild-type, *Kruppel-* and *twist-* embryos. Contrarily to the deformation in the AP axis (extension), most deformation in the DV axis is negative (convergence), except for a peak of cell shape changes caused by mesoderm invagination which overlaps with the first 10 minutes of germ-band extension. Consistent with this, the peak of positive tissue deformation in DV is present in wild-type and *Kruppel-* embryos (**A**, **B**), but not in *twist-* embryos (**C**). The ribbons for AP axis deformations are shaded, whereas those for DV axis deformations are not.

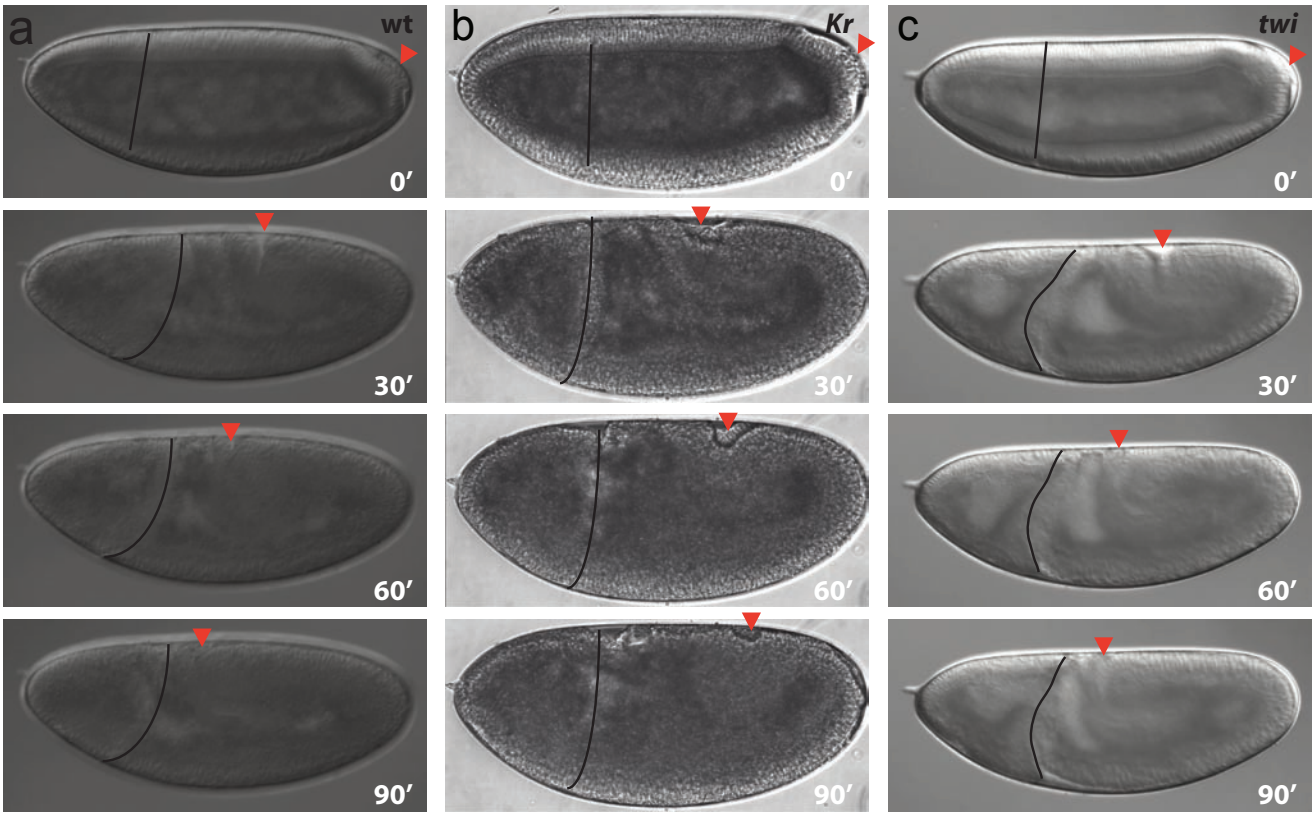


**Figure S2** Germ-band extension in wild-type, *Kruppel-* and *twist-* embryos. Frames of movies collected under Nomarski optics, showing lateral views of embryos from wild-type, *Krüppel-* and *twist-* embryos (anterior to the left, dorsal uppermost). The red arrow labels the position of the extending end of the germ-band (thus the extent of GBE), while the black line shows the position of the cephalic furrow. Whereas wild-type and *twist-* embryos have almost completely extended their germ-band after 90 minutes, *Krüppel-* embryos fail to complete extension. Note that the extension which remains in *Kruppel-* embryos takes place within the first 30 minutes of GBE.

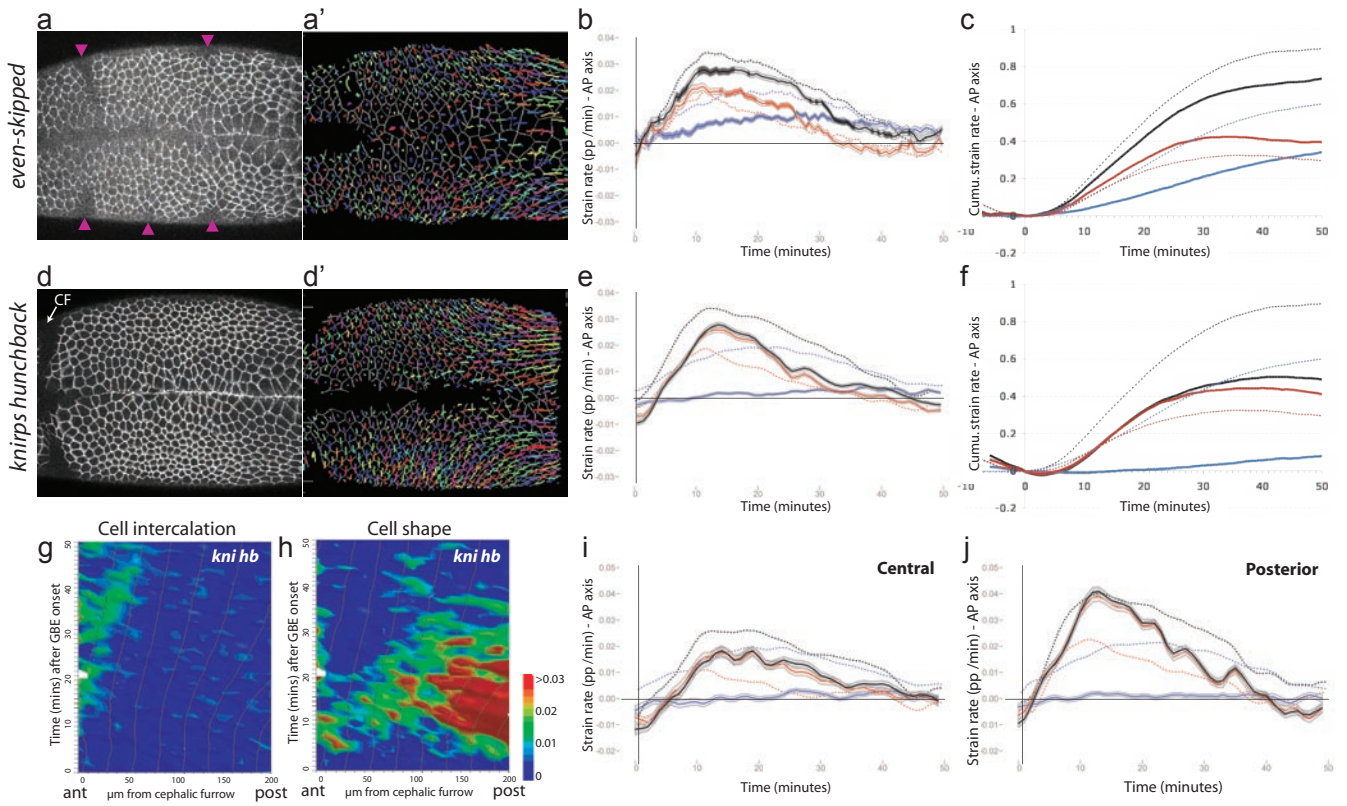


**Figure S3** Relative contribution of cell shape change and cell intercalation to germ-band extension in *even-skipped* **and** *knirps hunchback* mutant embryos. **(A**-**C**) Analysis of *even-skipped* (*eve*) mutant embryos**.** (**A**) Movie frame showing a projection of confocal sections through the cell apices labelled with *DEcadGFP* for a typical *eve* mutant embryo. *eve* mutants do not form a cephalic furrow (compare with D), but shallow folds form in the epithelium (arrowheads). A') Corresponding tracked movie frame, showing the cell lineages, cell centroids and cell outlines recorded by the tracking software. (**B**) Summary of tissue in the AP axis for 5 *eve* embryos, showing total (black), cell intercalation (blue) and cell shape (red) strain rates. Dotted lines show the wild-type data for comparison. The shaded sections of the ribbons indicate when a given cell behaviour in the mutant is significantly different from the equivalent at that time in wild-type ($p<0.05$). (**C**) Cumulative representation of the same data, accumulating from t=0. (**D**-**J**) Analysis of a single *knirps hunchback* (*kni hb*) mutant embryo. (**D**) Movie frame showing a projection of confocal sections through the cell apices labelled with *DEcadGFP*. The cephalic furrow (CF) is indicated with an arrow. (**D'**) Corresponding tracked movie frame. (**E**) Summary of tissue deformation in the AP axis for one *kni hb* embryo, showing total (black), cell intercalation (blue) and cell shape (red) strain rates. Dotted lines show the wild-type data for comparison. The statistical model used can not be applied to a sample size with a single embryo, hence ribbons are not colour-coded. (**F**) Cumulative representation of the same data, accumulating from t=0. (**G**, **H**) Strain rates for cell intercalation and cell shape contributing to tissue extension, in a *kni hb* embryo represented as a function of the cell's position along the AP axis. Strain rates are colour coded according to the scale shown (note that any values below 0 will be coded blue, while any above 0.03 will be coded red). (**I**, **J**) Strain rates in the AP axis for total (black), cell intercalation (blue) and cell shape (red), for the central and posterior populations of ectodermal cells in wild-type and a *kni hb* embryo. Wild-type is shown as dotted lines and *kni hb* as a ribbon.

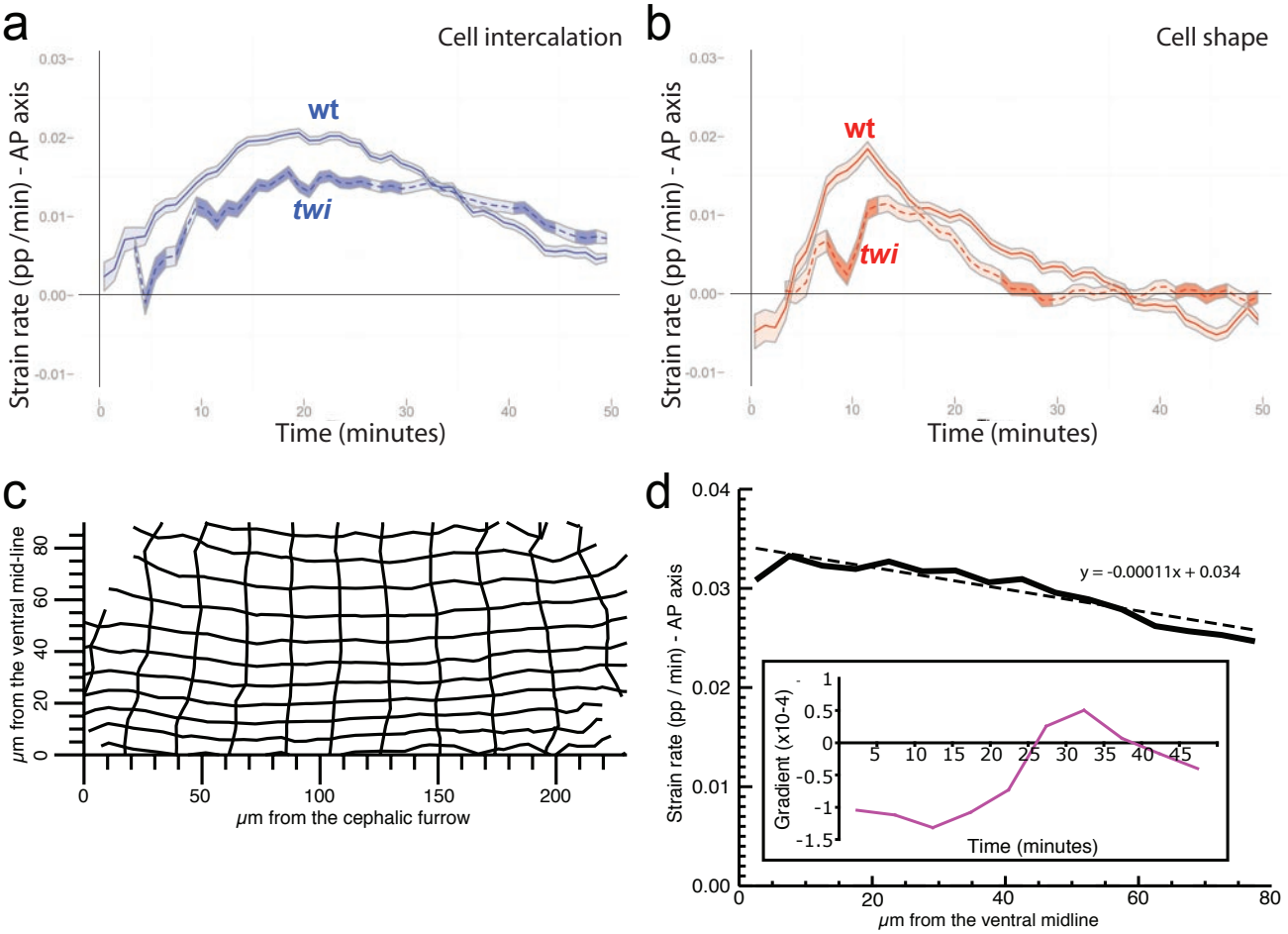


**Figure S4** Further analysis on *twist* mutant embryos. (**A**) Rate of cell intercalation in ectodermal cells for *twist*- embryos compared to wild-type. Ribbon shading indicates a significant difference between mutant and wild-type ($p<0.05$). (**B**) Similar analysis for the rate of cell shape changes. (**C**-**D**) Quantification of the difference in the rate of tissue extension between the midline and lateral ectoderm. (**C**) Representation of the tissue stretching occurring between 5 and 25 minutes of germ-band extension in wild-type embryos with respect to the two embryonic axes. For the AP axis, positions are given in µm from the cephalic furrow, which is located at the anterior edge of the field of view. For the DV axis, cell positions are given in µm from the midline that bisects the embryo (see Fig 1A, (**A'**). The tissue extends more axially (close to the midline) than laterally (away from the midline), as shown by the spacing between the vertical lines in the deformation grid: these are more widely spaced closer to the midline. (**D**) Rate of tissue deformation in wild-type embryos summarised over the same period (5 to 25 minutes of germ-band extension), as a function of cells position along the DV axis. This confirms that there is a gradient of deformation, with rate of deformation being highest for tissue close to the midline (black curve with best fit function shown as a dotted line). The inset shows the time evolution of this gradient: the gradient's slope is negative between 5 and 25 minutes, as shown in the above curve. This is the period of GBE when there is an axial bias in tissue deformation. At 25 minutes, this bias ceases, and then reverses, showing that between 25 and 40 minutes, the lateral tissue is now deforming faster than the midline tissue.

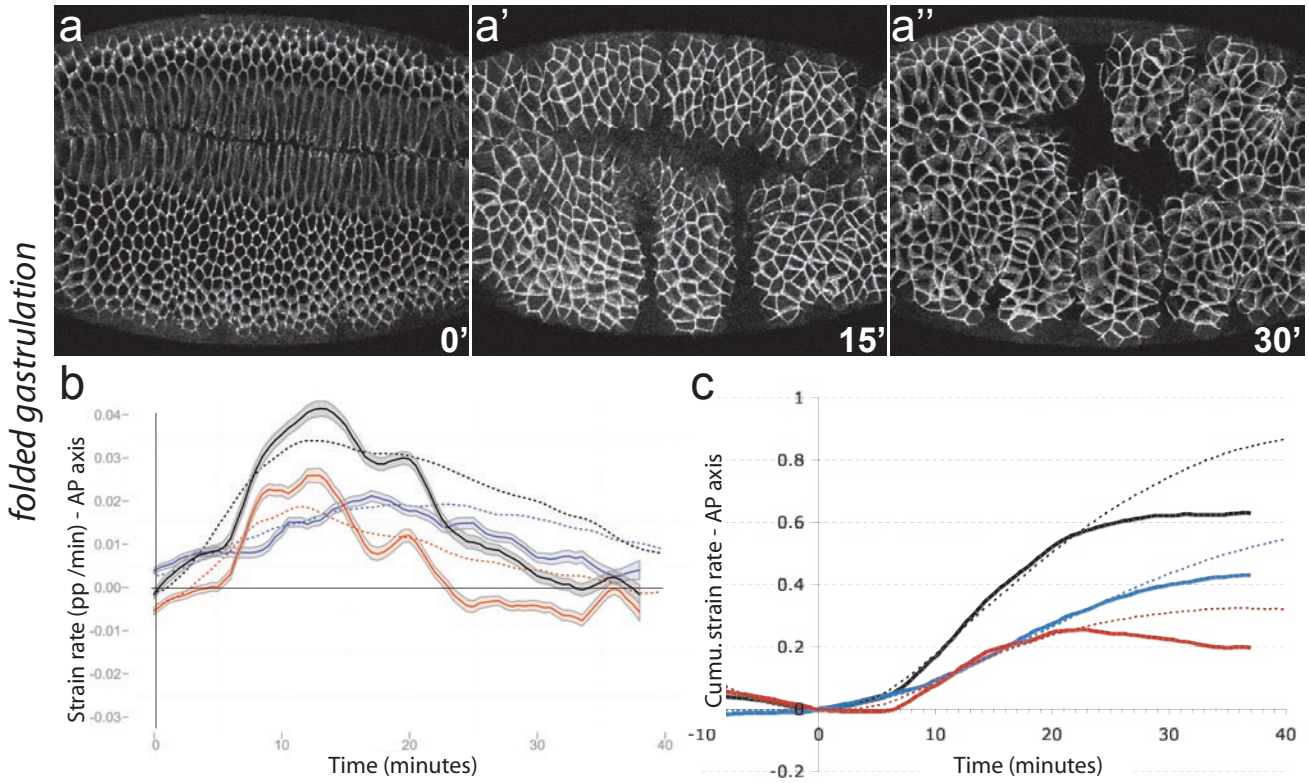


**Figure S5** Analysis of a *folded gastrulation* mutant. (**A-A"**) Movie frames showing the ventral side of a *folded gastrulation* mutant embryo. When germ-band extension starts (panel 0 minute), the embryo looks similar to a wild-type embryo. As the germ-band extends, folds form progressively perpendicular to the ventral mid-line, and the embryo starts to twist. The block in posterior midgut invagination, which forces the extending germ-band to buckle, causes this concertinaed phenotype. (**B**) Summary of tissue deformation in the AP axis for this embryo, showing total (black), cell intercalation (blue) and cell shape (red) strain rates. Ribbons are not colour-coded, since we cannot apply the statistical model to a sample size with a single embryo. Dotted lines show the wild-type data for comparison. (**C**) Cumulative representation of the same data, accumulating from t=0. Curves starts to deviate from wild-type (dotted lines) at around 20 minutes, when deformation curves are not comparable to those in wild-type embryos because *fog* embryos start twisting.

**Supplementary Movies Legends**

**Movie S1** Camera lucida cartoon of a small patch of extending lateral tissue, based on frames from a DECad-GFP confocal movie. This movie illustrates the complexity of the cell behaviours occurring during germ-band extension.

**Movie S2** Confocal DECad-GFP movie for a representative wild-type embryo.

**Movie S3** Confocal DECad-GFP movie for a representative *Kruppel-* embryo

**Movie S4** Confocal DECad-GFP movie for a representative *twist-*embryo

**Movie S5** Tracked movie for the wild-type embryo. Multicoloured tracks represent the trajectory of the centre of each cell over the previous 8 time-points (4 minutes).

**Movie S6** Tracked movie for the *Kruppel-* embryo. Multicoloured tracks represent the trajectory of the centre of each cell over the previous 8 time-points (4 minutes).

**Movie S7** Tracked movie for the *twist-* embryo. Multicoloured tracks represent the trajectory of the centre of each cell over the previous 8 time-points (4 minutes).

**Movie S8** Tissue deformation movie for the corresponding wild-type embryo. The positive strain rate vectors (indicating extension) are shown in blue, while the negative strain rate vectors (indicating convergence) are in red.

**Movie S9** Tissue deformation movie for the corresponding *Kruppel-* embryo. The positive strain rate vectors (indicating extension) are shown in blue, while the negative strain rate vectors (indicating convergence) are in red.

**Movie S10** Tissue deformation movie for the corresponding *twist-* embryo. The positive strain rate vectors (indicating extension) are shown in blue, while the negative strain rate vectors (indicating convergence) are in red.

**Movie S11** Cell shape deformation movie for the corresponding wild-type embryo

**Movie S12:** Cell shape deformation movie for the corresponding *Kruppel-* embryo

**Movie S13** Cell shape deformation movie for the corresponding *twist-* embryo

**Movie S14** Cell intercalation deformation movie for the corresponding wild-type embryo

**Movie S15** Cell intercalation deformation movie for the corresponding *Kruppel-* embryo

**Movie S16** Cell intercalation deformation movie for the corresponding *twist-* embryo